

Transition-Event Durations in One Dimensional Activated Processes

Bin W. Zhang and David Jasnow *

*Department of Physics & Astronomy,
University of Pittsburgh, Pittsburgh, Pennsylvania 15260*

Daniel M. Zuckerman †

*Department of Computational Biology, School of Medicine,
University of Pittsburgh, Pennsylvania 15213*

(Dated: 1st May 2019)

Abstract

Despite their importance in activated processes, transition-event durations — which are much shorter than first passage times — have not received a complete theoretical treatment. We therefore study the distribution $\rho_b(t)$ of durations of transition events over a barrier in a one-dimensional system undergoing over-damped Langevin dynamics. We show that $\rho_b(t)$ is determined by a Fokker-Planck equation with absorbing boundary conditions, and obtain a number of results, including: (i) the analytic form of the asymptotic short-time behavior ($t \rightarrow 0$), which is universal and independent of the potential function; (ii) the first non-universal correction to the short-time behavior; (iii) following Gardiner [1], a recursive formulation for calculating, exactly, all moments of ρ_b based solely on the potential function — along with approximations for the distribution based on a small number of moments; and (iv) a high-barrier approximation to the long-time ($t \rightarrow \infty$) behavior of $\rho_b(t)$. We also find that the mean event duration does not depend simply on the barrier-top frequency (curvature), but is sensitive to details of the potential. All of the analytic results are confirmed by transition-path-sampling simulations, implemented in a novel way.

* Electronic mail: jasnow@pitt.edu

† Electronic mail: dmz@ccb.pitt.edu

I. INTRODUCTION

Stochastic descriptions of dynamics have been invoked to describe protein folding [2], protein dynamics [3], chemical isomerization [4], and chemical reactions [5] among many other examples too numerous to list here. A Brownian particle moving in a one-dimensional bistable potential typically provides a model for chemical and biological reaction systems [6, 7, 8].

Basic aspects of the problem we address can be understood by examining Figs. 1 and 2, where we show a trajectory for a Brownian particle moving in a one-dimensional double-well potential. There are two timescales of interest, see [9]. One is the waiting time, or first passage time (FPT), which is the time the particle stays in one potential minimum before it goes to the other minimum. The other timescale is that for just climbing over the barrier separating the two minima, excluding the waiting time. We refer to this latter time as the “transition-event duration”; it has also been termed the “translocation time” in the context of membrane and pore traversal [10]. In the right hand graph of Fig. 1, one transition-event extracted from the full time series on the left is shown at higher temporal resolution. See also Fig. 2.

Theoretical analysis of the first passage time is largely a textbook subject now [1, 11]. In the simplest description, activated dynamics are modeled as Poisson processes, and the first passage time hence follow an exponential distribution. The mean FPT is given by Kramers’ theory [6, 9], and depends on the height of the barrier as well as the curvatures at the minimum and at the barrier top. More complex models of the FPT distribution have also been studied [12, 13].

Transition event durations have received focused attention only more recently [4, 10, 14, 15]. The event duration is important because it reflects the detailed dynamics of an activated transition. The statistics of event durations are of biological interest in many situations, such as transport in ion channels [10, 15, 16], polymer translocation through a pore [14, 17, 18, 19]. Recently developed nanosecond and femtosecond-scale experimental techniques [20, 21] have the potential to probe, directly, transition events. This short timescale is also fundamental to simulation techniques, such as path sampling [22, 23, 24, 25, 26, 27, 28, 29]; see also [30, 31, 32, 33, 34, 35, 36]. We further note that many previous theoretical treatments based on optimization of the Onsager-Machlup action

[37] discuss aspects of the transition event duration [38, 39, 40, 41, 42, 43, 44, 45, 46, 47]. Also, the distribution of transition paths is directly described in the work of Dykman and colleagues [48, 49, 50].

The transition-event duration may be defined in a simple way. In particular, Fig.2 shows that two positions are defined as the start and end points of the transition; usually they are on the different sides of a barrier. When a transition occurs, the event duration is the time interval between the last time the particle passes the start point and the first time it reaches the end point. Although arbitrary choices are inherently necessary for the start and end points, these do not appear to affect the basic physics.

The probability distribution of transition-event durations was previously studied in a phenomenological way by Zuckerman and Woolf [4]. Hummer [51] gives an analytic formula for the mean transition-event duration for an arbitrary one-dimensional potential. Indirectly, Redner's study of the first passage time in an interval supplies important precedents for our work [52], as does Gardiner's book [1]. Two groups have recently discussed the time-reversal symmetry of the ρ_b distribution, albeit without attempting the detailed probe of the distribution itself [10, 15], which we pursue here. Other efforts directed at polymer translocation [17, 18, 19] investigated a related but distinct problem, critically differing in boundary conditions; see Sec. IV.

In this work, we first review the derivation of the probability distribution of the transition-event durations, $\rho_b(t)$, from the Fokker-Planck Equation (FPE) with particular boundary conditions. We then obtain novel results. A recursive formula for all the moments of $\rho_b(t)$ is found, which permits accurate numerical approximations of ρ_b for an arbitrary potential. The short-time behavior of ρ_b is studied by path integral techniques, yielding universal behavior along with a potential-dependent correction. For a bistable potential with a high barrier (i.e. a "double-well"), the long time behavior of $\rho_b(t \rightarrow \infty)$ will be discussed.

II. BROWNIAN MOTION

Our description of transition-events will be based on the traditional approach of a one dimensional "reaction coordinate" x coupled to a thermal bath [27]. The analysis assumes over-damped Brownian dynamics, which we will variously address via a Langevin de-

scription, the associated Fokker-Planck equation and related path integral methods. In the following three subsections we introduce our notation, terminology, and the basic model.

The direct object of our study, the distribution of transition-event durations, will be fully introduced in Section IV.

A. Over-Damped Langevin Dynamics

We consider Brownian, stochastic dynamics as governed by the over-damped Langevin equation for a generalized coordinate x in the presence of Gaussian white noise [27],

$$\frac{dx}{dt} = \frac{F(x)}{\gamma} + R(t), \quad (1)$$

where

$$F(x) = -\frac{\partial U(x)}{\partial x}. \quad (2)$$

is the physical, systematic, conservative force acting on the particle, based on the potential energy U , and γ is the friction constant. In this work, the noise, $R(t)$, is taken to be Gaussian and white with zero mean and correlation

$$\langle R(t)R(t') \rangle = \left(\frac{2k_B T}{\gamma} \right) \delta(t - t'). \quad (3)$$

Here k_B is Boltzmann's constant, and T is the temperature.

Individual realizations of the noise in Eq.(1) generate stochastic trajectories $x(t)$, which are routinely simulated numerically as described in Section III.

B. Fokker-Planck Equation

To extract statistical information on trajectories one generally turns from the Langevin equation to the associated Fokker-Planck equation (FPE). The relation is discussed in standard monographs; see, for example [6]. The FPE describes the average behavior of a statistical ensemble of trajectories $x(t)$.

In one dimension the time evolution of the probability density function $P(x, t)$, for the

coordinate x is assumed to be described by the Fokker-Planck equation [1]

$$\frac{\partial P(x, t)}{\partial t} = \left[-\frac{\partial}{\partial x} D^{(1)}(x) + \frac{\partial^2}{\partial x^2} D^{(2)}(x) \right] P(x, t). \quad (4)$$

In Eq.(4), $D^{(2)}(x) > 0$ is the diffusion coefficient and $D^{(1)}(x)$, is the drift coefficient. When $D^{(2)} = k_B T / \gamma \equiv D$, with D the diffusion constant, and $D^{(1)}(x) = F(x) / \gamma$, this Fokker-Planck equation embodies the over-damped Langevin dynamics of Eq.(1) with noise correlation satisfying Eq.(3) [6]. In this simplified case we obtain

$$\frac{\partial P(x, t)}{\partial t} = -\frac{\partial}{\partial x} \left\{ -D \left[\frac{dU^*(x)}{dx} + \frac{\partial}{\partial x} \right] P(x, t) \right\}, \quad (5)$$

where $U^*(x) = U(x) / k_B T$ is the dimensionless physical potential. The solution of the Fokker-Planck equation under suitable initial and boundary conditions will allow statistical information to be extracted.

Eq.(5) clearly expresses conservation of probability. The total current associated with the stochastic variable x is given by [1]

$$J(x, t) = -D \left[\frac{dU^*(x)}{dx} + \frac{\partial}{\partial x} \right] P(x, t), \quad (6)$$

where the first term represents the drift (systematic) contribution, while the second term is the diffusion contribution.

C. Path Integral Approach

Path integral methods provide a useful tool and a different perspective for the study of Brownian motion [53, 54, 55]. Trajectories $x(t)$ are directly considered, rather than their average as in the FPE. The relative probability of a trajectory, $W[x(t)]$, connects the path integral back to the original Langevin equation (1). It can be shown that the relative probability for a Brownian particle described by the Langevin equation (1) to follow a specific path $x(\tau)$, with τ the time, is given by [53]

$$W[x(\cdot)] = \exp \left\{ -\frac{1}{4D} \int_{t_0}^t L[x(\tau)] d\tau \right\}, \quad (7)$$

where the effective Lagrangian can be expressed as

$$L[x(\tau)] = \left(\frac{dx}{d\tau} - \frac{F}{\gamma} \right)^2 + \frac{2D}{\gamma} \frac{dF}{dx}. \quad (8)$$

Then the optimal (classical) path $x_c(\tau)$ can be found in the standard fashion from the stationarity of the exponent “action”,

$$\delta \int_{t_0}^t L[x(\tau)] d\tau = 0, \quad (9)$$

with $x(t_0) = a$ and $x(t) = x$. Integrating over the probability densities of individual paths, the propagator

$$G(x, t|a, t_0) = \int_{a, t_0}^{x, t} W[x(\tau)] d[x(\tau)], \quad (10)$$

determines the probability of the particle arriving at position $x = x(t)$ at time t given that it started at $a = x(t_0)$. With a suitable definition of the measure in the integration in (10) the propagator is equivalent to the “principal solution” or Green function solution of the associated Fokker-Planck equation [53, 55].

When the diffusion coefficient D is small, the major contribution to the propagator will come from the paths very close to the optimal path $x_c(\tau)$. So, for $D \rightarrow 0$, the simplest approximation retains only the contribution from the optimal path [53], and is of the form

$$G(x, t|a, t_0) \cong K(t) \exp \left\{ -\frac{1}{4D} \int_{t_0}^t L[x_c(\tau)] d\tau \right\}, \quad (11)$$

where $K(t)$ is the normalizing factor to ensure the propagator satisfies

$$\int_{-\infty}^{\infty} G(x, t|a, t_0) dx = 1. \quad (12)$$

To include small fluctuations around the classical path, one typically invokes a quadratic approximation, in which deviations to second order are retained in the effective Lagrangian. Writing

$$x(\tau) = x_c(\tau) + \delta(\tau), \quad (13)$$

with $\delta(t_0) = \delta(t) = 0$, and neglecting terms in the Lagrangian higher than the second order

in δ , one finds [53]

$$G(x, t|a, t_0) = \exp\left(\frac{1}{2k_B T} \int_a^x F dx'\right) \left\{ 4\pi D [2E + 4DV(a)]^{\frac{1}{2}} [2E + 4DV(x)]^{\frac{1}{2}} \int_a^x (2E + 4DV(x'))^{-\frac{3}{2}} dx' \right\}^{-\frac{1}{2}} \\ \times \exp\left[-\frac{1}{4D} \int_{t_0}^t \left(\frac{dx_c}{d\tau}\right)^2 d\tau - \int_{t_0}^t V(x_c) d\tau\right]. \quad (14)$$

Here the effective potential, $V(x)$, (distinct from the physical potential U) is given by

$$V(x) = \frac{F(x)^2}{4k_B T \gamma} + \frac{1}{2\gamma} \frac{dF}{dx}. \quad (15)$$

The constant E in Eq.(14) is the “energy” of the particle, appearing as an integration constant in the first integral of the effective equation of motion following from the Lagrangian in Eq.(8) and the extremization in Eq.(9). The first integral yields the equation of motion,

$$\frac{dx_c}{d\tau} = \{2E + 4DV[x_c(\tau)]\}^{\frac{1}{2}}, \quad (16)$$

which is the equation for a classical particle of mass $\frac{1}{2}$ in the presence of a conservative potential $-2DV(x)$ [53]. Larger values of E give optimal solutions for increasingly more rapid events.

The quadratic approximation is justified if the path probability decreases sufficiently rapidly with increasing variation of the path from the optimal one [53]. This is expected in the limit of weak diffusion ($D \rightarrow 0$) in analogy with the semi-classical approximation in quantum mechanics with $\hbar \rightarrow 0$; see, e.g., [53].

The path integral approach provides some interesting insights for the features of Brownian dynamics of concern in this paper. We will return to this description below.

III. SIMULATION

All of our key analytic results to be discussed below have been confirmed via numerical simulation. Here our simulation approaches are briefly described.

A. Brute Force Simulation

Standard simulations of the over-damped Langevin Eq.(1) employ a simple first-order scheme with fixed time step Δt , such that

$$x_j = x(j\Delta t), \quad j = 0, 1, 2, \dots \quad (17)$$

and [8]

$$x_{j+1} = x_j + \frac{F(x_j)}{\gamma} \Delta t + \Delta x_R. \quad (18)$$

Consistent with Eq.(3) the thermal fluctuation (noise increment) Δx_R is chosen from a Gaussian distribution of zero mean and variance

$$\sigma^2 = 2 \left(\frac{k_B T}{\gamma} \right) \Delta t = 2D\Delta t. \quad (19)$$

However, as is well-known, this direct approach proves inadequate to simulate rare events, even in one dimension. A program running on a single CPU can provide an ensemble of transition trajectories (with thousands of transition-events) only for low barrier height. For high barriers, the waiting time between successful events will become unacceptably long. Therefore, we employed a path-sampling method for simulations, which we now describe.

B. Path Sampling

The problem with direct “brute force” simulations is that the waiting time between events grows exponentially with barrier height [11]. Our interest here, moreover, is to obtain a statistically well-sampled ensemble of transitions. In practice, for any given model, we require thousands of events.

To generate a sufficient quantity of transition-events, we turn to a Monte Carlo path-sampling approach. The approach has its roots in Path Integral Monte Carlo for quantum systems [56, 57], but Pratt provided an important advance in recognizing the analogous application in classical and, particularly, chemical systems [22].

Pratt’s approach has recently been taken up with some vigor by Chandler and co-

workers [24, 58]. Related work was presented by Zimmer and Paniconi [59, 60]. An independent path-sampling approach was developed by Zuckerman and Woolf [8, 25], building on work by Ottinger [61].

The basic idea of path-sampling is simple: focus computer time on the rare transition events of interest, Fig. 1(right), rather than on the waiting time between events, which can be longer by many orders of magnitude, Fig. 1(left). In a statistical mechanics context, the probability of a path can be computed. Hence “trial” paths can be included by means of re-weighting [8] or by a Metropolis criterion [24].

Here we primarily follow Pratt’s approach to path sampling, which is based on two facts: (i) Path (i.e., trajectory) probabilities are readily computed for stochastic processes, so that trajectories may be viewed as $N \times d$ dimensional equilibrium “objects”, when there are N time steps and d spatial dimensions. (ii) Wherever equilibrium probabilities can be computed for all such “objects” in a space, Metropolis sampling can be performed.

As in any Metropolis simulation, we require that detailed balance is satisfied. That is, for arbitrary paths i and j with equilibrium probabilities P and overall transition rates Γ , we require

$$P_{path}(i)\Gamma(i \rightarrow j) = P_{path}(j)\Gamma(j \rightarrow i). \quad (20)$$

The rate Γ is decomposed into the usual product of the generating (*gen*) and acceptance (*acc*) components [24, 62], which are proportional to the conditional probability for generating and accepting the trial path j , starting from i . Then trial moves should be accepted with probability $\min[1, R]$, where

$$R = \frac{acc(i \rightarrow j)}{acc(j \rightarrow i)} = \frac{P_{path}(j) \times gen(j \rightarrow i)}{P_{path}(i) \times gen(i \rightarrow j)}. \quad (21)$$

All paths in our ensemble will have the same total number of steps N , so that the probability of two paths can be compared via Eq.(21). We will typically choose N to be much bigger than $\langle t \rangle_b / \Delta t$, with $\langle t \rangle_b$ the mean time for transition events, so that the “full shape” of the distribution is sampled. Thus, transition events will typically constitute only part of N -step trajectories in our sample of paths. On the other hand, intentionally selecting N smaller than $\langle t \rangle_b / \Delta t$ when necessary allows us to focus on the short-time behavior of ρ_b .

To proceed, we must establish the equilibrium and generating probabilities in Eq.(21). The “equilibrium” probability P_{path} of the N -step path from a to x_N is the product of the equilibrium probability for the initial point and all subsequent single-step transition probabilities consistent with Eqs.(18) and (19). We further restrict our ensemble to “successful” paths containing transition events by formally introducing a projection operator θ . Thus we have

$$P_{path}(\{a, x_1, \dots, x_N\}) \propto \exp[-U^*(a)] \times [\prod_{i=0}^{N-1} p(x_i, x_{i+1}; U^*)] \times \theta(\{x_i\}). \quad (22)$$

The single-step transition probability corresponding to Eqs.(18) and (19) is a Gaussian density, namely

$$p(x_i, x_{i+1}; U^*) = \frac{1}{\sqrt{2\pi}\sigma} \exp \left\{ -\frac{\left[x_{i+1} - x_i - \frac{1}{2} \left(\frac{dU^*}{dx_i} \right) (2D\Delta t) \right]^2}{2\sigma^2} \right\}. \quad (23)$$

where $\frac{dU^*}{dx_i} \equiv \frac{dU^*(x)}{dx} \Big|_{x_i}$. If the particle returns to the left boundary a before arriving at the right boundary b , $\theta = 0$; otherwise $\theta = 1$.

We employ a novel path generating procedure designed to focus simulation effort on the distribution $\rho_b(t)$ of interest and, as necessary, on the rarest trial events. Our path generation strategy is closely related to a non-Metropolis re-weighting procedure previously considered by Zuckerman and Woolf [8]. Specifically, a trial path is built up “from scratch”, but based on the average behavior of the previous path. From the previous path, which starts from a and arrives at b after M_{old} ($M_{old} < N$) steps without being absorbed at a , we can calculate the average velocity over total time $M_{old}(2D\Delta t)$ as

$$\bar{v}(M_{old}) = \frac{b - a}{M_{old}(2D\Delta t)}. \quad (24)$$

This will be the “target speed” of the new trial path. This is extremely useful when studying the fastest events, whose transition-event durations are much shorter than $\langle t \rangle_b$.

To generate a new path, we linearly bias the particle from a to b using

$$x_{j+1} = x_j + (\bar{v}(M_{old}))(2D\Delta t) + \Delta x_R, \quad (25)$$

where Δx_R has been defined in Section III A following Eq(18). Eq.(25) may be compared to the unbiased form (18). The linear bias in (25) is motivated by the quasi-ballistic quality of the fastest transition-events deriving from Eq.(16) in the limit $E \gg DV_{max}$, where V_{max} is the maximum of $V(x)$ defined by Eq.(15). Thus, on the new path, the particle moves with a constant drift (bias) velocity, as if the force were constant, and ordinary noise. Note that for the new trajectory generated by Eq.(25), the new value, M_{new} , can be larger or smaller than M_{old} . Once it arrives at b , we remove the bias and allow the particle to move for the remainder of N steps as governed by unbiased Brownian motion Eq.(18). As noted above, all the paths must contain the same number of steps for probabilities to be compared in our Metropolis procedure using Eq.(21)

The generating probability (*gen*) for our procedure is the conditional probability with which we choose the new path, given the old one (with its average speed), namely,

$$gen(old \rightarrow new) = \prod_{i=0}^{M_{new}-1} \bar{g}(x_i, x_{i+1}; \bar{v}(M_{old})) \prod_{j=M_{new}}^{N-1} p(x_j, x_{j+1}; U^*), \quad (26)$$

where

$$\bar{g}(x_i, x_{i+1}, \bar{v}(M_{old})) = \frac{1}{\sqrt{2\pi\sigma}} \exp \left\{ -\frac{[x_{i+1} - x_i - (\bar{v}(M_{old}))(2D\Delta t)]^2}{2\sigma^2} \right\}. \quad (27)$$

This generating method is tailored to the potentials and boundary conditions we study in this paper, so that the Brownian particle will not be trapped in any position between the two absorbing walls.

By substituting Eqs.(22),(23),(26) and (27) into Eq.(21) we arrive at the acceptance criterion for our generating procedure, namely

$$R = \frac{\prod_{i=0}^{M_{new}-1} p(x_i, x_{i+1}, U^*) \theta_{new} \prod_{i=0}^{M_{old}-1} \bar{g}(y_i, y_{i+1}, \bar{v}(M_{new}))}{\prod_{i=0}^{M_{new}-1} \bar{g}(x_i, x_{i+1}, \bar{v}(M_{old})) \theta_{old} \prod_{i=0}^{M_{old}-1} p(y_i, y_{i+1}, U^*)}, \quad (28)$$

given an old transition path $(a, y_1, y_2, \dots, y_{M_{old}}, y_{M_{old}+1}, \dots, y_N)$ and a trial transition path $(a, x_1, x_2, \dots, x_{M_{new}}, x_{M_{new}+1}, \dots, x_N)$.

To ensure the correct behavior of our procedure and code, path-sampling results were carefully checked against direct simulation, using Eq.(18), in a number of cases. In the following sections of the paper, all the simulation results employ the path-sampling method just described.

We also checked that our path-sampling simulations greatly exceeded the correlation time resulting from our use of the “old” average velocity in Eq.(24). This resulted in negligible statistical uncertainty, as can be gauged from the smoothness of the data in all path-sampling figures.

IV. TRANSITION-EVENTS

A. Distribution of Transition-Event Duration

The distribution of transition-event durations, $\rho_b(t)$, for a Brownian particle confined to one dimension can be found by solving the Fokker-Planck equation using suitable boundary conditions, as we now describe [14].

During the entire transition process the particle must move between a and b , which means that only trajectories that stay completely within the interval are considered, i.e. $a \leq x(t) \leq b$ during the entire event. To eliminate the extraneous trajectories, absorbing walls must be put at the start and end points, [14], so that

$$\begin{aligned} P(a, t) &= 0 \\ P(b, t) &= 0. \end{aligned} \tag{29}$$

As recently stressed by Berezhkovskii [10], et al., the dual absorbing boundary conditions distinguish the event duration as a “conditional first passage time”, rather than the usual unconditional time associated with the Kramers’ problem [9, 10]. This contrasts with several previous studies of polymer translocation [10, 18, 19].

One releases particles very close to the left absorbing wall at $t = 0$, so that the initial condition is

$$P(x, 0) = \delta[x - (a + \epsilon)], \tag{30}$$

with $\epsilon \rightarrow 0+$. Then the current at the right absorbing wall will determine the distribution, ρ_b , of durations according to

$$\rho_b(t) \propto \lim_{\epsilon \rightarrow 0+} J(b, t), \tag{31}$$

with the currents given in Eq.(6). Following Gardiner’s work [1], let $\pi_b(a + \epsilon|t)$ equal the

probability that a particle, released at $a + \epsilon$, is absorbed at the right absorbing wall during $0 < \tau < t$. It is easy to see that

$$\pi_b(a + \epsilon|t) = \int_0^t J(b, \tau) d\tau. \quad (32)$$

If we define

$$\Pi_b(a + \epsilon) \equiv \pi_b(a + \epsilon|\infty) = \int_0^\infty J(b, \tau) d\tau, \quad (33)$$

this ‘‘splitting probability’’ can be used to normalize $\rho_b(t)$ in Eq.(31) according to

$$\rho_b(t) = \lim_{\epsilon \rightarrow 0^+} \frac{J(b, t)}{\int_0^\infty J(b, \tau) d\tau} = \lim_{\epsilon \rightarrow 0^+} \frac{J(b, t)}{\Pi_b(a + \epsilon)}. \quad (34)$$

We note that the splitting probabilities are time-independent and follow directly from the potential U^* according to [1, 51]:

$$\begin{aligned} \Pi_a(x) &= \frac{\int_x^b \exp[U^*(x')] dx'}{\int_a^b \exp[U^*(x')] dx'} \\ \Pi_b(x) &= \frac{\int_a^x \exp[U^*(x')] dx'}{\int_a^b \exp[U^*(x')] dx'} = 1 - \Pi_a(x). \end{aligned} \quad (35)$$

Hence, to find the distribution of the transition-event durations, $\rho_b(t)$, one must solve the Fokker-Planck equation (5) with the initial condition (30) and absorbing boundary conditions (29). The current, $J(b, t)$, can be found from Eq.(6), which can then be combined with the splitting probabilities to find the normalized distribution of transition-event durations, $\rho_b(t)$.

B. Examples: Free Diffusion and Linear Potential

The solution of the Fokker-Planck equation can be formally expressed, in standard fashion, in terms of the eigenvalues and eigenfunctions of a time independent equation [11]. The solution can be written in the form

$$P(x, t) = \sum_n A_n p_n(x) e^{-\lambda_n t}, \quad (36)$$

where the eigenvalues $\{\lambda_n\}$ are non-negative and, based on Eq.(5), the eigenfunctions satisfy

$$D \left\{ \frac{d}{dx} \left[\frac{dU^*(x)}{dx} \right] + \frac{d^2}{dx^2} \right\} p_n(x) = -\lambda_n p_n(x). \quad (37)$$

Eq.(37) with boundary conditions (29) determine the functions $\{p_n(x)\}$, while the constants $\{A_n\}$ are found from the initial condition (30). The distribution $\rho_b(t)$ follows from Eqs.(34) and (35). As examples, we determine $\rho_b(t)$ for a few special potentials $U^*(x)$. This will reveal some interesting features. We note that the linear potential, of which free diffusion is a special case, previously was studied by Lubensky and Nelson [14], although without numerical simulations.

Free Diffusion. Even in the absence of a true barrier, the event duration is still well defined by the formalism above, and this simple case acts as a useful reference. We therefore first consider free diffusion, with $U^*(x) = 0$ and $a = 0, b = L$.

The solution of Eq.(37) can easily be found, and the result can be formally expressed as

$$\rho_b^{(0)}(t) = 2D \sum_{j=1}^{\infty} (-1)^{j+1} \left(\frac{j\pi}{L} \right)^2 \exp\left(-\frac{j^2\pi^2}{L^2}Dt\right). \quad (38)$$

Notice that at long times the decay is exponential and dominated by the lowest eigenvalue.

The right-hand side of Eq.(38) is well behaved for long time, but is not useful for $t \rightarrow 0$. We can re-cast the result in a format useful at short times by using the Poisson sum formula [63],

$$\sum_{n=-\infty}^{\infty} f(n) = \sum_{j=-\infty}^{\infty} \int_{-\infty}^{\infty} f(x) \exp(-2i\pi jx) dx, \quad (39)$$

for function f . We then find an alternative representation

$$\rho_b^{(0)}(t) = \frac{2L}{\sqrt{\pi Dt^3}} \sum_{j=0}^{\infty} \left[\frac{(2j+1)^2 L^2 - 2Dt}{4Dt} \right] \exp\left[-\frac{(2j+1)^2 L^2}{4Dt} \right], \quad (40)$$

which can be used to extract the behavior as $t \rightarrow 0$, namely $\rho_b^{(0)}(t) \sim t^{-5/2} \exp[-L^2/(4Dt)]$. We note that Eq.(40) can also be derived using an image method, as described below in Section IV E 4.

Linear Potential. The solution for the linear potential, $U^*(x) = kx$, which corresponds to a constant drift velocity, can also be formally written in terms of an eigenfunction

expansion [14],

$$\rho_b(t) = 2D \sum_{j=1}^{\infty} (-1)^{j+1} \left(\frac{j\pi}{L} \right)^2 \left[\frac{\sinh(kL/2)}{kL/2} \right] \exp \left\{ -\frac{[(kL/2)^2 + j^2\pi^2]Dt}{L^2} \right\}. \quad (41)$$

Comparing with Eq.(38), the result can be written

$$\rho_b(t) = \rho_b^{(0)}(t) \left[\frac{\sinh(kL/2)}{kL/2} \right] \exp \left[-\frac{(kL/2)^2 Dt}{L^2} \right]. \quad (42)$$

In the left graph of Fig. 3 we show path-sampling simulation results following Section III B for ρ_b for free diffusion with $U^* = 0, L = 1.0$ and $U^* = 0, L = 2.0$. They are compared with the numerical evaluations of Eq.(38). The path-sampling simulations and numerical results from the eigenfunction expansions match very well. We changed the units of the vertical and horizontal axes, so that all the curves of $\rho_b^{(0)}$ will not depend on the width L , and the generic behavior is highlighted.

In the right graph of Fig. 3 we show path-sampling simulation results for a series of parameterizations of linear potential: $U^* = 4.0x, L = 2.0, U^* = 8.0x, L = 1.0, U^* = 9.0x, L = 2.0$, and $U^* = 18.0x, L = 1.0$, which are compared to numerical evaluation of Eq.(41). The simulation and numerical results again match very well. We again scaled the axes to emphasize that the shape of ρ_b only depends on the value of kL , which is essentially the potential energy difference between the start and end points. These exercises add confidence to the path-sampling methods used here.

C. Approximate Solution for Inverted Parabolic Potential

As a first investigation of a more realistic potential, we employ a crude representation of absorbing boundary conditions. In Fig. 4, inverted parabolic potentials are shown, one with open boundary conditions and the other with two absorbing walls ($U^* \rightarrow -\infty$; see, e.g., [11]). When the “barrier” is high i.e., when $U^*(0) \gg U^*(a = -1) = U^*(b = 1)$, a particle exiting the region $a < x < b$, has a small likelihood of returning with open boundary conditions, because of the rapidly increasing “downhill” forces external to the region. Thus, as long as there is a sufficiently high barrier, one might conclude the solution for open boundary conditions will be a good approximation for an inverted

parabolic potential with two absorbing walls. We now investigate this approximation.

With open boundary conditions, the exact solution of the Fokker-Planck equation for an inverted parabolic potential, $U^* = -\frac{1}{2}\alpha x^2$, is well known [11]:

$$P(x, t) = \sqrt{\frac{\alpha}{2\pi[1 - \exp(-2\alpha Dt)]}} \exp\left\{-\frac{\alpha[x \exp(-\alpha Dt) - a]^2}{2[1 - \exp(-2\alpha Dt)]}\right\} \exp(-\alpha Dt), \quad (43)$$

which satisfies the initial condition

$$P(x, 0) = \delta(x - a). \quad (44)$$

For the same potential with absorbing walls at $-W$ and W , we approximate the current from Eqs.(43) and (6) with $a = -W$ and $b = W$,

$$J(W, t) = \left(\frac{D\alpha W}{4} \sqrt{\frac{\alpha}{\pi}}\right) \frac{\exp[-(\alpha W^2/2) \coth(\alpha Dt/2)]}{\sinh(\alpha Dt/2) \sqrt{\sinh(\alpha Dt)}}. \quad (45)$$

For normalization we will need

$$N = \int_0^\infty J(W, t') dt', \quad (46)$$

which is the total probability passing to the right of $x = W$. Under the influence of this inverted parabolic potential, this probability will not pile up but will flow toward $x \rightarrow \infty$.

Thus

$$N = \Pi_\infty(-W) = \frac{\int_{-\infty}^{-W} \exp(-\frac{1}{2}\alpha x^2) dx}{\int_{-\infty}^{\infty} \exp(-\frac{1}{2}\alpha x^2) dx} = \frac{\text{erfc}(W \sqrt{\alpha/2})}{2}, \quad (47)$$

from which one obtains the approximation

$$\rho_b(t) \simeq \left\{ \frac{D\alpha W}{2[1 - \text{erf}(W \sqrt{\alpha/2})]} \right\} \left(\sqrt{\frac{\alpha}{\pi}} \right) \frac{\exp[-(\alpha W^2/2) \coth(\alpha Dt/2)]}{\sinh(\alpha Dt/2) \sqrt{\sinh(\alpha Dt)}}, \quad (48)$$

where $\text{erf}(x) = 1 - \text{erfc}(x) = \frac{2}{\sqrt{\pi}} \int_0^x \exp(-z^2) dz$ [64]. In Fig. 5 we compare the results from direct simulation and from Eq.(48) for inverted parabolic potentials with different heights. In the simulations the two absorbing walls are placed at $a = -1.0$ and $b = 1.0$; then the height of the barrier is given by $\alpha/2$.

As expected, this approximation improves with increasing barrier height.

D. Moments of the Distribution of Transition-Event Durations

1. Recursive Formula

In studying a distribution, it is natural to investigate its moments. Gardiner [1] provides an expression for the first moment of $\rho_b(t)$ (i.e., the mean time), which is also given by Hummer [51]. Here we derive a recursive formula for all *moments* of $\rho_b(t)$, as suggested by Gardiner [1].

Following Gardiner, we define $g_b(x, t)$ as the total probability that the particle is absorbed at b after time t , given that it is released at position x at $t = 0$. Thus

$$g_b(x, t) \equiv \int_t^\infty J(b, \tau) d\tau, \quad (49)$$

and we have the initial condition

$$P(x', 0) = \delta(x' - x). \quad (50)$$

The limiting cases for $g_b(x, t)$ are

$$\begin{aligned} g_b(x, t = 0) &= \Pi_b(x) \\ g_b(x, t = \infty) &= 0, \end{aligned} \quad (51)$$

where $\Pi_b(x)$ is defined in Eq.(35).

The n th moment, T_n , of the exit time distribution for particles released at arbitrary $a < x < b$ can be calculated from $g_b(x, t)$ according to

$$T_n(b, x) = - \int_0^\infty t^n \frac{\partial}{\partial t} \left[\frac{g_b(x, t)}{g_b(x, 0)} \right] dt = \frac{n}{\Pi_b(x)} \int_0^\infty t^{n-1} g_b(x, t) dt, \quad (52)$$

so that $T_n(b, a)$ is the n th moment of ρ_b . Gardiner [1] shows that $g_b(x, t)$ satisfies the

backward Fokker-Planck equation

$$\left(-D\frac{dU^*}{dx}\right)\frac{\partial g_b(x,t)}{\partial x} + D\frac{\partial^2 g_b(x,t)}{\partial x^2} = \frac{\partial g_b(x,t)}{\partial t}. \quad (53)$$

Multiplying by nt^{n-1} on both sides and integrating with respect to t yields

$$\left(-D\frac{dU^*}{dx}\right)\left[n\int_0^\infty t^{n-1}\frac{\partial g_b(x,t)}{\partial x}dt\right] + D\left[n\int_0^\infty t^{n-1}\frac{\partial^2 g_b(x,t)}{\partial x^2}dt\right] = n\int_0^\infty t^{n-1}\frac{\partial g_b(x,t)}{\partial t}dt. \quad (54)$$

Now the right side can be integrated by parts to find

$$n\int_0^\infty t^{n-1}\frac{\partial g_b(x,t)}{\partial t}dt = -n\Pi_b(x)T_{n-1}(b,x), \quad (55)$$

and with Eq.(52),

$$\left(-D\frac{dU^*}{dx}\right)\frac{dy(x)}{dx} + D\frac{d^2y(x)}{dx^2} = -n\Pi_b(x)T_{n-1}(b,x), \quad (56)$$

where

$$y(x) \equiv \Pi_b(x)T_n(b,x). \quad (57)$$

The boundary conditions on $y(x)$ are

$$y(b) = y(a) = 0. \quad (58)$$

One way to solve equations like (56) uses Green's functions [65]. The function that satisfies the homogeneous equation corresponding to Eq.(56) with boundary condition (58) at a is, in fact, $\Pi_a(x)$; correspondingly at b , it is $\Pi_b(x)$. Using these solutions, one obtains a recursive formula for all the moments

$$T_n(b,x) = \frac{n}{D}\left\{\int_a^b \exp[U^*(x')]dx'\right\}\left\{\frac{\Pi_a(x)}{\Pi_b(x)}\int_a^x \exp[-U^*(x')]\Pi_b^2(x')T_{n-1}(b,x')dx'\right. \\ \left. + \int_x^b \exp[-U^*(x')]\Pi_a(x')\Pi_b(x')T_{n-1}(b,x')dx'\right\}. \quad (59)$$

Our main interest is in the moments of ρ_b , namely,

$$T_n(b, a) = \frac{n}{D} \left\{ \int_a^b \exp[U^*(x)] dx \right\} \left\{ \int_a^b \exp[-U^*(x)] \Pi_a(x) \Pi_b(x) T_{n-1}(b, x) dx \right\}. \quad (60)$$

Given the moments according to Eq.(60), the distribution of transition-event durations, $\rho_b(t)$, can be reconstructed numerically, at least for a fixed range of t .

2. Lowest Eigenvalue

From Eqs.(6) and (36) one knows that $\rho_b(t)$ can be written in the series

$$\rho_b(t) = \sum_{n=1}^{\infty} C_n e^{-\lambda_n t}, \quad (61)$$

where the eigenvalues defined by Eq.(37) satisfy $0 < \lambda_1 < \lambda_2 < \lambda_3 < \dots$. The eigenvalues, in particular λ_1 , can be found via direct numerical solution of Eq.(37). Here we show an alternative based on integrations involving the potential. The first eigenvalue λ_1 can be expressed in terms of the high-order moments because of asymptotically exponential behavior. When $n \gg 1$,

$$\begin{aligned} T_n(b, a) &= \int_0^{\infty} t^n \rho_b(t) dt \\ &= \Gamma(n+1) \frac{C_1}{\lambda_1^{n+1}} \left[1 + \frac{C_2}{C_1} \left(\frac{\lambda_1}{\lambda_2} \right)^{n+1} + \frac{C_3}{C_1} \left(\frac{\lambda_1}{\lambda_3} \right)^{n+1} + \dots \right], \end{aligned} \quad (62)$$

where $\Gamma(n)$ is the Gamma function. The lowest eigenvalue can then be estimated from a ratio of high moments; for example,

$$\lambda_1 = \lim_{n \rightarrow \infty} \left[\frac{T_n(b, a)}{T_{n+1}(b, a)} (n+1) \right], \quad (63)$$

and from Eq.(62), the constant can be determined according to

$$C_1 = \lim_{n \rightarrow \infty} \frac{T_n(b, a) \lambda_1^{n+1}}{\Gamma(n+1)}. \quad (64)$$

Recalling that the moments can be constructed via successive integration, Eq.(63) provides a way to estimate the first eigenvalue in Eq.(61). In Section IV F Eq.(63) will be used together with simulations to check an approximate analytic result for the leading eigenvalue in a representative case.

3. First Moment

For $n = 1$, using $T_0(b, a) = 1$, Eq.(60) yields the first moment of the distribution of transition-event durations,

$$T_1(b, a) = \frac{1}{D} \left\{ \int_a^b \exp[U^*(x)] dx \right\} \left\{ \int_a^b \exp[-U^*(x)] \Pi_a(x) \Pi_b(x) dx \right\}. \quad (65)$$

We can immediately evaluate T_1 for the simple potentials. For free diffusion with $U^* = 0$ and $a = 0, b = L$,

$$\frac{2DT_1^0}{L^2} = \frac{1}{3}. \quad (66)$$

With $U^* = kx, a = 0, b = L$,

$$\frac{2DT_1}{L^2} = \frac{2}{(kL)^2} \left[kL \coth\left(\frac{kL}{2}\right) - 2 \right]. \quad (67)$$

For an inverted parabolic potential $U^* = H(1 - \frac{x^2}{W^2})$, where the curvature $\alpha = \frac{2H}{W^2}$, and $a = -W, b = W$, we can find an approximation of T_1 . When $H \gg 1$, by using the method of steepest descents,

$$\int_{-W}^W \exp[U^*(x)] dx \approx \exp(H) \sqrt{\frac{2\pi}{\alpha}}, \quad (68)$$

and

$$\Pi_a(x) \Pi_b(x) \approx \frac{1 - \left[\operatorname{erf}\left(\frac{x\sqrt{\alpha}}{\sqrt{2}}\right) \right]^2}{4}. \quad (69)$$

Then

$$\begin{aligned} 2DT_1 &\approx \sqrt{\frac{2\pi}{\alpha}} \int_0^W \exp\left(\frac{Hx^2}{W^2}\right) \left\{ 1 - \left[\operatorname{erf}\left(\frac{\sqrt{H}x}{W}\right) \right]^2 \right\} dx \\ &= \frac{\sqrt{\pi}W^2}{H} \int_0^{\sqrt{H}} \exp(y^2) \{1 - [\operatorname{erf}(y)]^2\} dy \end{aligned}$$

$$\begin{aligned}
&= \frac{\sqrt{\pi}W^2}{H} \left\{ \int_0^1 \exp(y^2)\{1 - [\text{erf}(y)]^2\}dy + \int_1^{\sqrt{H}} \exp(y^2)\{1 - [\text{erf}(y)]^2\}dy \right\} \\
&\approx \frac{W^2}{H} [1.27 + \log(H)] = \frac{2}{\alpha} [1.27 + \log(H)]. \tag{70}
\end{aligned}$$

Eq.(70) provides a good approximation for T_1 for the inverted parabolic potential with high barrier. It also gives a rough estimate of T_1 for a “single-bump” barrier with height H and width $2W$.

Naively, one might guess T_1 should simply be proportional to the effective frequency for the barrier top, namely, the inverse curvature α^{-1} . However, this intuition falls short in two respects. First, the logarithmic term in Eq.(70) is dominant for large barriers, even for this simplest purely parabolic potential. Further, in extensive numerical work, for a double-well potential, we have seen unambiguously that the mean event duration is sensitive to details of the potential far from the barrier top (data not shown). This sensitivity can be traced to the dependence of the optimal “speed”, Eq.(16), on details of the potential. To give an extreme example, if there were a second barrier and minimum in the potential, then T_1 would have to include the Kramers’ time for the second barrier.

4. Reconstruction of ρ_b from Moments

Reconstructing a function approximately from a finite number of moments has been studied, e.g., by maximum entropy method [66, 67, 68], continued fraction approach [69, 70], and Talenti method [71, 72] and perhaps other techniques. Here we follow Hon and Wei’s work [72] to reconstruct the density $\rho_b(t)$ in a similar way.

First one builds up an orthonormal set of basis functions $\psi_j(t)$, which are polynomials,

$$\psi_j(t) = \sum_{n=0}^j c_{jn} t^n, \tag{71}$$

by using the standard Gram-Schmidt orthonormalization technique [65]. The polynomials satisfy

$$\int_0^\infty \psi_{j'}(t)\psi_j(t)w(t)dt = \delta_{jj'}, \tag{72}$$

with respect to a weight function $w(t)$, which is tailored to our problem with the choice

$$w(t) = \exp(-\lambda_1 t) \exp\left(-\frac{L^2}{4Dt}\right) (1 + t^{-\frac{5}{2}}), \quad (73)$$

where $L = b - a$. For this weight factor, when $t \rightarrow \infty$, $w(t) \sim \exp(-\lambda_1 t)$, and when $t \rightarrow 0$, $w(t) \sim \exp\left(-\frac{L^2}{4Dt}\right) t^{-\frac{5}{2}}$. These forms represent the long-time and short-time behaviors for $\rho_b(t)$ as we will show in Section IV F and (IV E 4) below. Thus we built in all the information we know about $\rho_b(t)$ in this weight factor. Notice that λ_1 can be found by following the scheme in Section IV D 2, or via other numerical methods.

Following the usual Gram-Schmidt procedure, one builds up

$$\rho_m(t) = w(t) \sum_{j=0}^m a_j \psi_j(t), \quad (74)$$

which will be an approximation for $\rho_b(t)$ of “order” m . If we incorporate moments of ρ_b by setting coefficients according to

$$\begin{aligned} a_0 &= \frac{T_0}{\int_0^\infty \psi_0(t) w(t) dt} = \frac{1}{c_{00} \int_0^\infty w(t) dt} \\ a_j &= \frac{T_j - \sum_{i=0}^{j-1} a_i \int_0^\infty t^j \psi_i(t) w(t) dt}{\int_0^\infty t^j \psi_j(t) w(t) dt}, \end{aligned} \quad (75)$$

then $\rho_m(t)$ will reproduce the first m moments T_n ($0 \leq n \leq m$), i.e.,

$$T_n \equiv \int_0^\infty t^n \rho_b(t) dt \approx \int_0^\infty t^n \rho_m(t) dt. \quad (76)$$

By using the first five moments, we reconstruct the distribution of transition-event durations for several different double-well potentials. Two of the results are shown in Fig. 6. They match well with the simulations except for the long time tail as seen in the semi-log plot. However, the event probability in that region is quite small.

E. Short Time Behavior

Beyond the moments, it is of interest to study the asymptotic behavior of the event-duration distribution, in both short and long time limits. We first analyze the $t \rightarrow 0$ behavior, using exact methods.

1. Short Time Behavior for the Green Function with Open Boundary Conditions

From the perspective of the path integral, introduced in Section II C, if $(t - t_0)$ is short, the velocity on the optimal trajectory $\frac{dx_c}{dt}$ will be large. This implies a large “energy” E in Eq.(14). We therefore assume $2E \gg 4DV$ and obtain the corresponding Green function for short time t with open boundary conditions,

$$G(x, t|a, t_0) \approx \exp\left(\frac{1}{2k_B T} \int_a^x F dx'\right) \frac{1}{\sqrt{4\pi D(t - t_0)}} \exp\left[-\frac{(x - a)^2}{4D(t - t_0)}\right] \times \exp[-\bar{V}(t - t_0)], \quad (77)$$

where \bar{V} is the average effective potential between a and x ,

$$\bar{V} = \frac{1}{x - a} \int_a^x V(x') dx'. \quad (78)$$

We have used the quadratic approximation, which is expected to be reasonable if the diffusion coefficient D is small [53]. Also, because we are further restricting our analysis to short-time behavior, the important paths will be close to the optimal one, which should improve the approximation.

If we define G_0 as the Green function for free diffusion with open boundary conditions [1],

$$G_0(x, t|a, t_0) = \frac{1}{\sqrt{4\pi D(t - t_0)}} \exp\left[-\frac{(x - a)^2}{4D(t - t_0)}\right], \quad (79)$$

Eq.(77) can be expressed as

$$G(x, t|a, t_0) \approx G_0(x, t|a, t_0) \exp\left(\frac{1}{2k_B T} \int_a^x F dx'\right) \exp[-\bar{V}(t - t_0)], \quad (80)$$

which will be useful when we discuss the early time behavior with alternative boundary

conditions below in Section IV E 2.

2. Short Time Behavior for the Current with Absorbing Boundary Conditions

In this subsection we need to retrace the path integral method in order to study transition-event durations, as required, with two absorbing walls.

As shown in Fig. 7, we wish to calculate the path integral from the start point '+' at $x = 0+$ to the end point 'o' at $x = L-$ during the time interval $(t - t_0)$. There are two absorbing walls at position $x = 0$ and $x = L$, with some arbitrary potential between them. If the position of the start point is ϵ_1 and the end point is x , then the Green function G^{abs} with absorbing boundary conditions can be expressed as a sum over Green functions G for open boundary conditions [54]

$$G^{abs}(x, t|\epsilon_1, t_0) = \sum_{j=-\infty}^{\infty} G(2jL + x, t|\epsilon_1, t_0) - \sum_{j=-\infty}^{\infty} G(2jL - x, t|\epsilon_1, t_0). \quad (81)$$

The construction is shown schematically in Fig. 7.

As shown above, to determine the distribution of event durations, we first calculate the current at x , then take the limits $\epsilon_1 \rightarrow 0$ and $x \rightarrow L$,

$$J^{abs}(L, t|0, t_0) = -2D \sum_{j=-\infty}^{\infty} \left. \frac{\partial G(x, t|0, t_0)}{\partial x} \right|_{x=(2j+1)L}. \quad (82)$$

From Eq.(80), when $(t - t_0)$ is small

$$\begin{aligned} \left. \frac{\partial G(x, t|0, t_0)}{\partial x} \right|_{x=(2j+1)L} &\approx \left. \frac{\partial G_0(x, t|0+, t_0)}{\partial x} \right|_{x=(2j+1)L} \times \exp \left[\frac{1}{2k_B T} \int_0^{(2j+1)L} F dx' \right] \\ &\times \exp[-\bar{V}_j(t - t_0)], \end{aligned} \quad (83)$$

where the symmetry of the periodically continued potential has been used; see Fig. 7.

The periodicity implies further simplifications, including

$$\int_0^{(2j+1)L} F dx' = \int_0^L F dx'$$

$$\bar{V}_j = \frac{1}{(2j+1)L} \int_0^{(2j+1)L} V(x') dx' = \frac{1}{L} \int_0^L V(x') dx' = \bar{V}_0. \quad (84)$$

If we define the free diffusion current with absorbing boundary conditions as

$$J_0^{abs}(L, t|0, t_0) = -2D \sum_{j=-\infty}^{\infty} \left. \frac{\partial G_0(x, t|0, t)}{\partial x} \right|_{x=(2j+1)L}, \quad (85)$$

Eq.(82) can be written

$$J^{abs}(L, t|0, t_0) \approx J_0^{abs}(L, t|0, t_0) \exp\left(\frac{1}{2k_B T} \int_0^L F dx'\right) \exp[-\bar{V}_0(t - t_0)], \quad (86)$$

or

$$J^{abs}(b, t|a, t_0) \approx J_0^{abs}(b, t|a, t_0) \exp\left(\frac{1}{2k_B T} \int_a^b F dx'\right) \exp[-\bar{V}(t - t_0)] \quad (87)$$

where

$$\bar{V} = \frac{1}{b-a} \int_a^b V(x') dx'. \quad (88)$$

We can now estimate the short time behavior of the normalized current.

3. Short Time behavior for the distribution of the transition-event durations

Combining Eq.(34) and (87), we find that the short-time behavior for the distribution of transition-event durations is given by

$$\rho_b(t \rightarrow 0) \approx \rho_b^{(0)}(t) \exp\left(\frac{1}{2k_B T} \int_a^b F dx'\right) \exp(-\bar{V}t) \left[\lim_{\epsilon \rightarrow 0^+} \frac{\Pi_b^0(a + \epsilon)}{\Pi_b(a + \epsilon)} \right], \quad (89)$$

where $\Pi_b^0(x)$ is the splitting probability for free diffusion and $\rho_b^{(0)}$ is the distribution for free-diffusion with absorbing boundary conditions. From Eq.(35)

$$\lim_{\epsilon \rightarrow 0^+} \frac{\Pi_b^0(a + \epsilon)}{\Pi_b(a + \epsilon)} = \frac{\int_a^b \exp[U^*(x')] dx'}{\exp[U^*(a)](b-a)}. \quad (90)$$

Combining Eq.(89) and (90), and using $F(x) = k_B T \left(-\frac{dU^*}{dx}\right)$, the normalized distribution becomes

$$\rho_b(t \rightarrow 0) \approx \rho_b^{(0)}(t) \left\{ \frac{\int_a^b \exp[U^*(x')] dx'}{\exp[U^*(a)](b-a)} \right\} \exp \left[\frac{U^*(b) - U^*(a)}{2} \right] \exp(-\bar{V}t), \quad (91)$$

revealing corrections to the free diffusion result due to the potential.

In Fig. 8 we compare the results from a path-sampling simulation as described in Sec. III B and our final result Eq.(91) for two double-well potentials of varying barrier height. The simulations and the analytic results of Eq.(91) are in good agreement at sufficiently early times, although at the earliest times the simulations reveal degrading statistics.

4. Comment on the Short Time Behavior of $\rho_b^{(0)}(t)$

For the free diffusion problem with absorbing walls, the path integral method in Section IV E 2 can give the solution. Redner [52] shows that an image method, similar to that used in electromagnetism, will give the same result

$$\rho_b^{(0)}(t) = \frac{2L}{\sqrt{\pi Dt^3}} \sum_{j=0}^{\infty} \left[\frac{(2j+1)^2 L^2 - 2Dt}{4Dt} \right] \exp \left[-\frac{(2j+1)^2 L^2}{4Dt} \right]. \quad (92)$$

If $Dt \ll L^2$,

$$\rho_b^{(0)}(t) \sim t^{-\frac{3}{2}} \exp \left(-\frac{L^2}{4Dt} \right). \quad (93)$$

Eq.(93) shows the short time behavior of ρ_b for free diffusion with absorbing boundary conditions. Combining it with Eq.(91), one can find the short time behavior in the presence of the potential.

F. Long Time Behavior for Double-Well Potential

From Eqs.(6) and (36) we know that the long time behavior of $\rho_b(t)$ will be determined primarily by the first eigenvalue λ_1 . Here we use a perturbative approach to obtain an approximation for λ_1 for a double-well potential with high barrier. We confirm, by

direct numerical calculation, the validity of using perturbation theory. We also perform path-sampling simulations to check the accuracy of our final approximation.

By a variable transformation, the one dimensional Fokker-Planck equation can be transformed to a Schrödinger-like equation [11]. If we let $\phi_n(x) = \exp(\frac{U^*}{2})p_n(x)$, Eq.(37) becomes

$$\left[-D \frac{d^2}{dx^2} + V_s(x) \right] \phi_n(x) = \lambda_n \phi_n(x), \quad (94)$$

where

$$V_s(x) = \frac{D}{4} \left(\frac{dU^*(x)}{dx} \right)^2 - \frac{D}{2} \frac{d^2 U^*(x)}{dx^2}, \quad (95)$$

which is exactly the effective potential in Eq.(15). The eigenvalue spectrum remains the same [11].

We write a double-well potential in the form

$$U^* = H \left[1 - \left(\frac{x}{W} \right)^2 \right]^2, \quad (96)$$

where H is the height of the barrier in units of $k_B T$ and W is the half-width of the barrier. We will consider double-wells having high barriers, $H \gg 1$, and fixed half width, W . The absorbing walls are placed at the two minima, $x = \pm W$. The Schrödinger potential corresponding to (96) is

$$V_s(x) = D \left[\frac{2H}{W^2} + \left(\frac{4H^2}{W^4} - \frac{6H}{W^4} \right) x^2 - \frac{8H^2}{W^6} x^4 + \frac{4H^2}{W^8} x^6 \right]. \quad (97)$$

In Fig.9 we plot $U^*(x)$ and $V_s(x)$ for a double-well with sufficiently high barrier. For the potential in the Schrödinger picture, $V_s = +\infty$ outside the central interval to ensure the wave functions $\phi_n(x)$ vanish at the ends of the interval, thus satisfying the absorbing boundary conditions.

We use perturbation theory to describe the lowest stationary state, which must exist because of the boundary conditions. For sufficiently high barriers, we expect that, the lowest eigenstate will be localized at the central minimum, suggesting the use of a perturbation process based on a simple harmonic oscillator. Using a numerical procedure for bound-state solutions of the time-independent Schrödinger equation [73], we confirmed this localization for high barriers. We also note that for high barriers, the oscillator's

Gaussian wave function nearly vanishes at the boundaries, in approximate satisfaction of the proper boundary conditions.

Our perturbation calculation is therefore based on separating off the dominant harmonic component of V_s , noting $H \gg 1$, using

$$V_s(x) = V_0(x) + V_1(x), \quad (98)$$

where

$$V_0(x) = D \left(\frac{2H}{W^2} + \frac{4H^2}{W^4} x^2 \right), \quad (99)$$

$$V_1(x) = D \left(-\frac{6H}{W^4} x^2 - \frac{8H^2}{W^6} x^4 + \frac{4H^2}{W^8} x^6 \right). \quad (100)$$

From textbook results for a linear harmonic oscillator, the first eigenvalue and wave function are

$$\lambda_1^{(0)} = D \left(\frac{4H}{W^2} \right), \quad (101)$$

$$\psi_1^{(0)}(x) = \frac{\sqrt{\gamma}}{\pi^{1/4}} \exp\left(-\frac{1}{2}\gamma^2 x^2\right), \quad (102)$$

where

$$\gamma = \left(\frac{2H}{W^2} \right)^{1/2}. \quad (103)$$

The first order perturbative correction is

$$\lambda_1^{(1)} = \int \psi_1^{(0)*} V_1(x) \psi_1^{(0)} dx = D \left[-\frac{3}{W^2} + \mathcal{O}\left(\frac{1}{HW^2}\right) \right], \quad (104)$$

which is down by a factor of H from the zero order result. The second order correction is down by another factor of H :

$$\lambda_1^{(2)} = \sum'_m \left\{ \frac{|V_{m1}|^2}{\lambda_1^{(0)} - \lambda_m^{(0)}} \right\} \sim D \left[\mathcal{O}\left(\frac{1}{HW^2}\right) \right]. \quad (105)$$

The net result for the lowest eigenvalue is thus

$$\lambda_1 = D \left[\frac{4H}{W^2} - \frac{3}{W^2} + \mathcal{O}\left(\frac{1}{HW^2}\right) \right] \quad (106)$$

$$= D \left[\alpha - \frac{3}{W^2} + \mathcal{O}\left(\frac{1}{HW^2}\right) \right], \quad (107)$$

where $\alpha = 4H/W^2$ gives the curvature at the top of the barrier.

Eq.(107) shows that the long time behavior is simply linear in the barrier-top curvature α , for large values of α and fixed W . This is also the case for the inverted parabolic potential, as can be determined from Eq.(48), or by performing the same calculation as we did for the double-well in this section. In fact, when $Dt\alpha \gg 1$, Eq.(48) becomes

$$\rho_b(t) \simeq \left[\frac{D\alpha W}{1 - \operatorname{erf}(W\sqrt{\alpha/2})} \right] \left(\sqrt{\frac{2\alpha}{\pi}} \right) \exp\left(-\frac{\alpha W^2}{2}\right) \exp(-D\alpha t). \quad (108)$$

We therefore expect similar linearity with α in the higher barrier limit for any system that can be approximated by an inverted parabola and a high order correction.

We performed numerical checks of the approximation (107). We determined the lowest eigenvalue λ_1 numerically using high moments and Eq.(63). We also used path-sampling simulations as a consistency check. Fig. 10 compares the numerical evaluation of λ_1 via Eqs.(63) and (64) with a path-sampling simulation data for a particular double-well potential.

In Fig. 11, we compare Eq.(107) with numerical calculations of λ_1 for double-well potentials and inverted parabolae with fixed W and a range of curvatures (10 – 100) and plot $\lambda_1/D\alpha$ as a function of curvature αW^2 . As Eq.(107) predicts, $\lambda_1/D\alpha$ approaches unity for large curvature.

V. SUMMARY

We have applied a combination of analytic and numerical techniques to study the distribution, $\rho_b(t)$, of the durations of transition-events over a barrier in a one-dimensional system undergoing over-damped Langevin dynamics. The typical event duration is much shorter than the well-studied first passage time (FPT) [10]; see Figs. 1 and 2. The event duration scale is the simplest non-trivial measure of the detailed dynamics of an activated

process, and we believe it is critical for future quantitative study of dynamics of many chemical and biological systems [4].

The distribution $\rho_b(t)$ can be derived from the Fokker-Planck equation with special boundary conditions and was subjected to detailed analysis. A number of results are obtained, including: (i) the analytic form of the asymptotic short-time behavior ($t \rightarrow 0$), which is universal and independent of the potential function; (ii) the first non-universal correction to the short-time behavior; (iii) following Gardiner [1], a recursive formulation for calculating, exactly, all moments of ρ_b based solely on the potential function — along with approximations for the distribution based on a small number of moments; (iv) a high-barrier approximation to the long-time ($t \rightarrow \infty$) behavior of $\rho_b(t)$; and (v) a rough but simple analytic estimate of the average event duration $\langle t \rangle_b$, which generally is sensitive to details of the potential. All of the analytic results are confirmed by transition-path-sampling simulations.

A number of interesting questions remain open. Perhaps most centrally, what changes in ρ_b can be expected for high-dimensional system with potentially “rough” and complex landscapes. A particular interest is in conformational transitions in proteins [74]. Furthermore, it is relevant to consider how non-white noise affect event durations. Finally, how can the detailed relationship between ρ_b and first passage-time be quantified, if at all?

ACKNOWLEDGMENTS

We are grateful to Profs. Marty Ytreberg, Joseph Rudnick, Daniel Boyanovsky, Vladimir Savinov and Mark Dykman for their interest and helpful comments and communications. It also a pleasure to thank Drs. Arun Setty, Ed Lyman, and Svetlana Aroutiounian for helpful discussions. This work was supported in part by the NIH Grant GM070987 to DMZ.

-
- [1] C. Gardiner, *Handbook of stochastic methods for physics, chemistry, and the natural sciences*, 2nd ed. (Springer-Verlag, 1994).
- [2] A. Naganathan, J. Sanchez-Ruiz, and V. Munoz, *J. Am. Chem. Soc.* **127**, 17970 (2005).
- [3] B. Isralewitz, M. Gao, and K. Schulten, *Curr.Opin.Struct.Biol.* **11**, 224 (2001).
- [4] D. M. Zuckerman and T. B. Woolf, *J. Chem. Phys.* **116**, 2586 (2002).
- [5] V. N. Smelyanskiy *et al.*, *J. Chem. Phys.* **110**, 11488 (1999).
- [6] R. Zwanzig, *Nonequilibrium Statistical Mechanics*, 1st ed. (Oxford University Press, USA, 2001).
- [7] H. C. Berg, *Random Walks in Biology*, 1st ed. (Princeton Univ Pr, 1993).
- [8] D. M. Zuckerman and T. B. Woolf, *J. Chem. Phys.* **111**, 9475 (1999).
- [9] P. Hänggi, P. Talkner, and M. Borkovec, *Rev. Mod. Phys.* **62**, 251 (1990).
- [10] A. M. Berezhkovskii, G. Hummer, and S. M. Bezrukov, *Phys. Rev. Lett.* **97**, 020601 (2006).
- [11] H. Risken, *Fokker-Planck Equation: Methods of Solution and Applications*, 2nd ed. (Springer-Verlag, 1989).
- [12] M. E. Fisher and A. B. Kolomeisky, *Proc. Natl. Acad. Sci. U. S. A.* **96**, 6597 (1999).
- [13] G. Margolin and E. Barkai, *Phys. Rev. E* **72**, 025101 (2005).
- [14] D. K. Lubensky and D. R. Nelson, *Biophys. J.* **77**, 1824 (1999).
- [15] J. Alvarez and B. Hajek, *Phys. Rev. E* **73**, 046126 (2006).
- [16] I.-C. Yeh and G. Hummer, *Proc. Natl. Acad. Sci. U. S. A.* **101**, 12177 (2004).
- [17] W. Sung and P. J. Park, *Phys. Rev. Lett.* **77**, 783 (1996).
- [18] M. Muthukumar, *J. Chem. Phys.* **111**, 10371 (1999).
- [19] M. Muthukumar, *Phys. Rev. Lett.* **86**, 3188 (2001).
- [20] J. Herbst, K. Heyne, and R. Diller, *Science* **297**, 822 (2002).
- [21] E. Samoylova *et al.*, *J. Am. Chem. Soc.* **127**, 1782 (2005).
- [22] L. R. Pratt, *J. Chem. Phys.* **85**, 5045 (1986).
- [23] R. Olender and R. Elber, *J. Chem. Phys.* **105**, 9299 (1996).
- [24] C. Dellago, P. G. Bolhuis, and D. Chandler, *J. Chem. Phys.* **108**, 9236 (1998).
- [25] T. B. Woolf, *Chem. Phys. Lett.* **289**, 433 (1998).
- [26] R. Elber, J. Meller, and R. Olender, *J. Phys. Chem. B* **103**, 899 (1999).
- [27] D. M. Zuckerman and T. B. Woolf, *Phys. Rev. E* **63**, 016702 (2000).

- [28] P. Eastman, N. Gronbeck-Jensen, and S. Doniach, *J. Chem. Phys.* **114**, 3823 (2001).
- [29] P. G. Bolhuis, D. Chandler, C. Dellago, and P. L. Geissler, *Annu. Rev. Phys. Chem.* **53**, 291 (2002).
- [30] M. Berkowitz, J. D. Morgan, J. A. McCammon, and S. H. Northrup, *J. Chem. Phys.* **79**, 5563 (1983).
- [31] R. Czerminski and R. Elber, *J. Chem. Phys.* **92**, 5580 (1990).
- [32] C. Choi and R. Elber, *J. Chem. Phys.* **94**, 751 (1991).
- [33] S. Fischer and M. Karplus, *Chem. Phys. Lett.* **194**, 252 (1992).
- [34] S. Huo and J. E. Straub, *J. Chem. Phys.* **107**, 5000 (1997).
- [35] R. Crehuet and M. J. Field, *J Chem Phys* **118**, 9563 (2003).
- [36] S. A. Trygubenko and D. J. Wales, *J. Chem. Phys.* **120**, 2082 (2004).
- [37] L. Onsager and S. Machlup, *Phys. Rev.* **91**, 1505 (1953).
- [38] M. Dykman and M. Krivoglaz, *Sov. Phys. JETP* **50**, 30 (1979).
- [39] A. J. Bray and A. J. McKane, *Phys. Rev. Lett.* **62**, 493 (1989).
- [40] M. I. Dykman, *Phys. Rev. A* **42**, 2020 (1990).
- [41] A. J. McKane, H. C. Luckock, and A. J. Bray, *Phys. Rev. A* **41**, 644 (1990).
- [42] A. J. Bray, A. J. McKane, and T. J. Newman, *Phys. Rev. A* **41**, 657 (1990).
- [43] H. C. Luckock and A. J. McKane, *Phys. Rev. A* **42**, 1982 (1990).
- [44] A. J. Mckane, *J. Phys. A* **26**, 5629 (1993).
- [45] R. Olender and R. Elber, *J. Mol. Struct.: THEOCHEM* **398-399**, 63 (1997).
- [46] M. Bier, I. Derényi, M. Kostur, and R. D. Astumian, *Phys. Rev. E* **59**, 6422 (1999).
- [47] R. Elber and D. Shalloway, *The Journal of Chemical Physics* **112**, 5539 (2000).
- [48] M. I. Dykman, P. V. E. McClintock, V. N. Smelyanski, N. D. Stein, and N. G. Stocks, *Phys. Rev. Lett.* **68**, 2718 (1992).
- [49] M. I. Dykman, D. G. Luchinsky, P. V. E. McClintock, and V. N. Smelyanskiy, *Phys. Rev. Lett.* **77**, 5229 (1996).
- [50] M. I. Dykman and V. N. Smelyanskiy, *Superlattices Microstruct.* **23**, 495 (1998).
- [51] G. Hummer, *J. Chem. Phys.* **120**, 516 (2004).
- [52] S. Redner, *A guide to first-passage processes*, 1st ed. (Cambridge University Press, 2001).
- [53] F. Wiegand, *Introduction to path-integral methods in physics and polymer science*, 1st ed. (World Scientific Publishing Co Pre Ltd, 1986).

- [54] H. Kleinert, *Path Integrals in Quantum Mechanics, Statistics, and Polymer Physics, and Financial Markets*, 3rd ed. (World Scientific Pub Co Inc, 2004).
- [55] L. S. Schulman, *Techniques and Applications of Path Integration*, 1st ed. (John Wiley & Sons Inc, 1981).
- [56] E. L. Pollock and D. M. Ceperley, *Phys. Rev. B* **30**, 2555 (1984).
- [57] D. M. Ceperley and E. L. Pollock, *Phys. Rev. Lett.* **56**, 351 (1986).
- [58] C. Dellago, P. G. Bolhuis, F. S. Csajka, and D. Chandler, *J. Chem. Phys.* **108**, 1964 (1998).
- [59] M. F. Zimmer, *Phys. Rev. Lett.* **75**, 1431 (1995).
- [60] M. Paniconi and M. F. Zimmer, *Phys. Rev. E* **59**, 1563 (1999).
- [61] H. C. Ottinger, *Macromolecules* **27**, 3415 (1994).
- [62] D. Frenkel and B. Smit, *Understanding Molecular Simulation: From Algorithms to Applications*, 2nd ed. (Academic Pr, 2001).
- [63] E. W. Weisstein, *Poisson Sum Formula* (MathWorld—A Wolfram Web Resource, <http://mathworld.wolfram.com/PoissonSumFormula.html>).
- [64] E. W. Weisstein, *Error Function* (MathWorld—A Wolfram Web Resource, <http://mathworld.wolfram.com/Erf.html>).
- [65] G. B. Arfken and H. J. Weber, *Mathematical methods for physicists*, 5th ed. (Harcourt/Academic Press, 2001).
- [66] L. R. Mead and N. Papanicolaou, *J. Math. Phys.* **25**, 2404 (1984).
- [67] A. Tagliani, *J. Math. Phys.* **34**, 326 (1993).
- [68] D. Poland, *J. Chem. Phys.* **102**, 2604 (1995).
- [69] M. S. Jhon and J. S. Dahler, *J. Chem. Phys.* **68**, 812 (1978).
- [70] A. Macchi, A. A. Maradudin, and V. Tognetti, *Phys. Rev. B* **53**, 5363 (1996).
- [71] G. Talenti, *Inverse Probl.* **3**, 501 (1987).
- [72] Y. C. Hon and T. Wei, *Eng. Anal. Bound. Elem.* **26**, 855 (2002).
- [73] H. Gould and J. Tobochnik, *An Introduction to Computer Simulation Methods : Applications to Physical System*, 2nd ed. (Addison Wesley, 1995).
- [74] D. M. Zuckerman, *J. Phys. Chem. B* **108**, 5127 (2004).

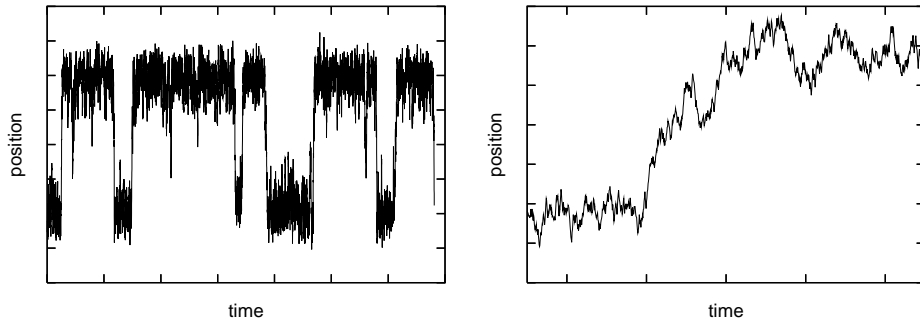


Figure 1: Trajectory for a Brownian particle moving in a double well potential. The left graph is a long trajectory with several transition-events. The right graph is the detail of a single transition-event cut from the same long trajectory.

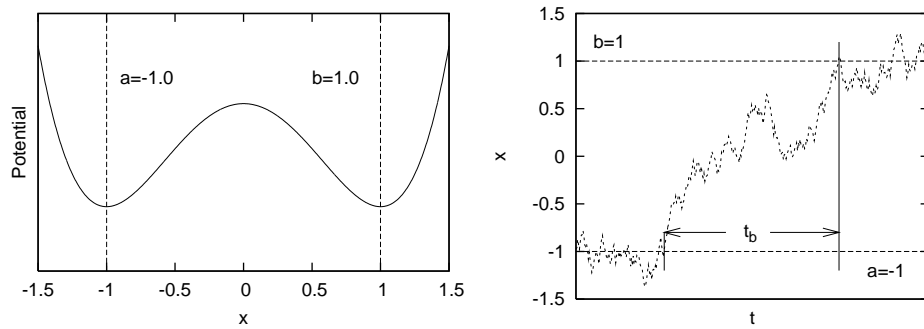


Figure 2: The definition of transition-event duration. In the left graph, two positions are defined as the start point a and end point b of the transition. For a transition-event in the right graph, transition-event duration is the duration between last time the particle passes a and the first time it passes b .

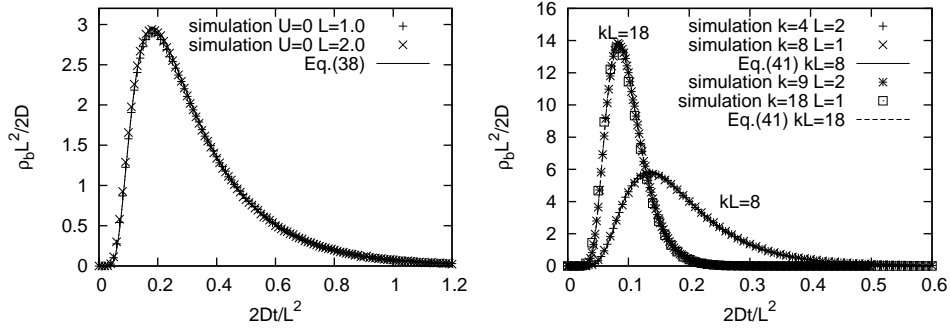


Figure 3: Scaled event duration distribution for free diffusion and the linear potential. The left graph is for free diffusion with different widths L , where data points are from path-sampling simulations and numerical evaluations of Eq.(38). The right graph is for the potential $U^* = kx$ with different widths L and different slopes k ; the points are data from path-sampling simulations and the lines are numerical evaluations of Eq.(41).

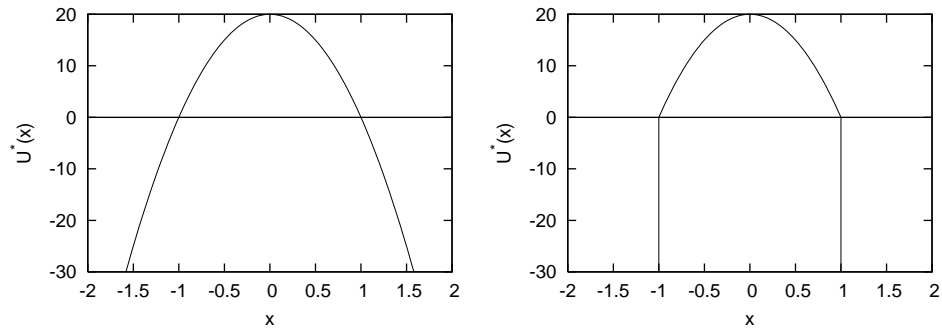


Figure 4: Inverted parabolic potential with different boundary conditions. The left graph is the inverted parabolic potential $U^* = -20(1 - x^2)$, with open boundary condition. The right graph is the same potential with two absorbing walls at $x = -1$ and $x = 1$.

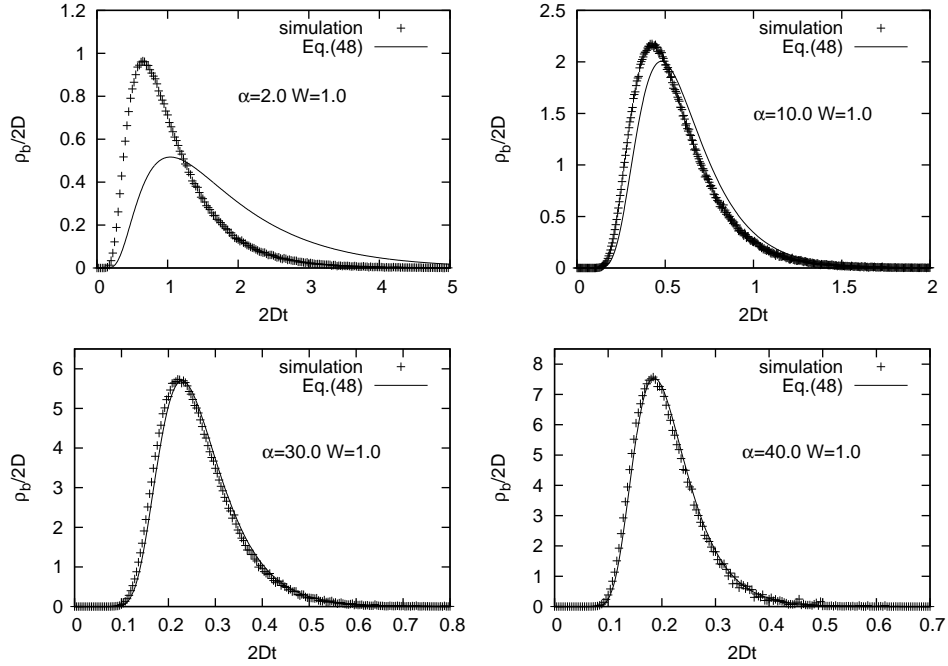


Figure 5: The event-duration distribution ρ_b for inverted parabolic potentials with different dimensionless barrier heights $\frac{\alpha}{2}$. The absorbing walls are at $-W$ and W , with $W = 1$. The data are from path-sampling simulation and numerical evaluations (lines) use the approximate formula, Eq.(48). This approximation improves with increasing barrier height.

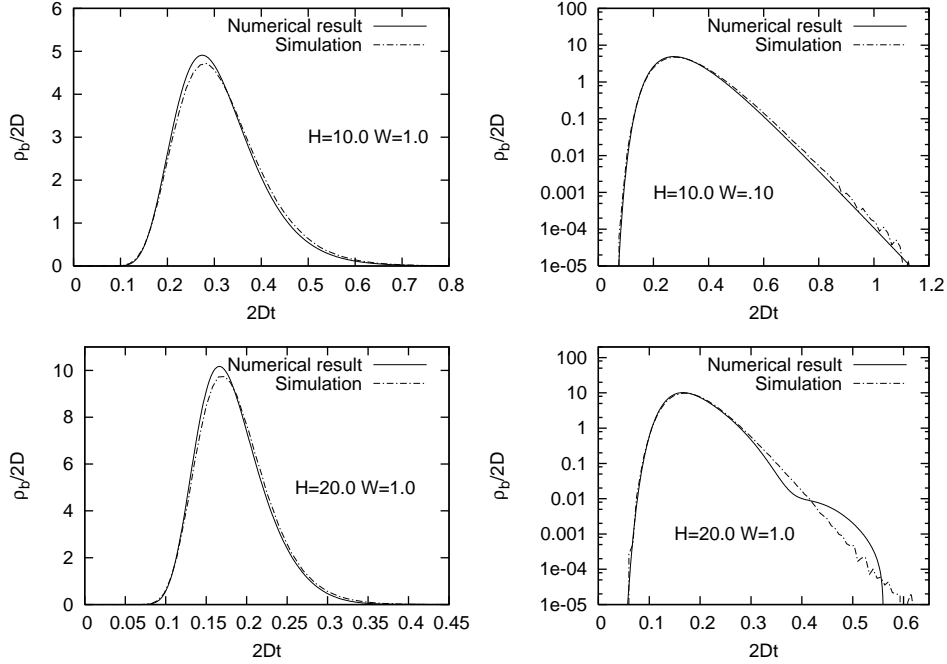


Figure 6: Reconstruction of ρ_b for double-well potentials $U^* = H \left[\left(\frac{x}{W} \right)^2 - 1 \right]^2$ based on moments and a Gram-Schmidt procedure. The two absorbing walls are at $-W$ and W , where $W = 1$. The data are from path-sampling simulations and numerical results are based on theory in Section IV D 1 and IV D 4, using the first five moments. They match well except the long time tail as emphasized in the semi-log plot.

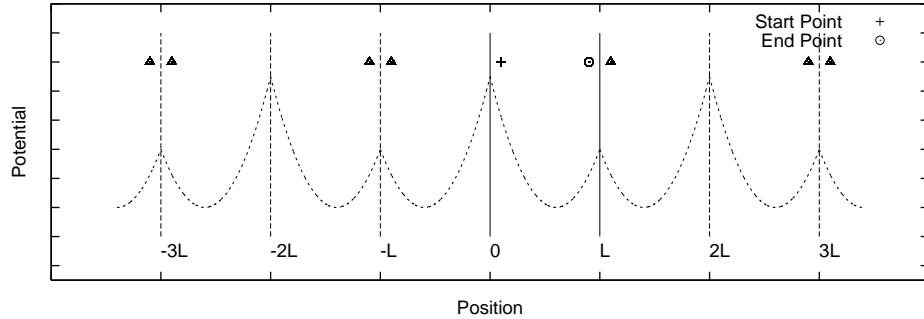


Figure 7: Calculating the path integral between the start point '+' and the end point 'o' with absorbing walls at $x = 0$ and $x = L$. The dashed curve represents an arbitrary potential between the two absorbing walls. Eq.(81) indicates that one must calculate the path integrals between the start point '+' and all "end points", including the real one 'o' and image end points ' Δ ', in the periodic potential with open boundary condition.

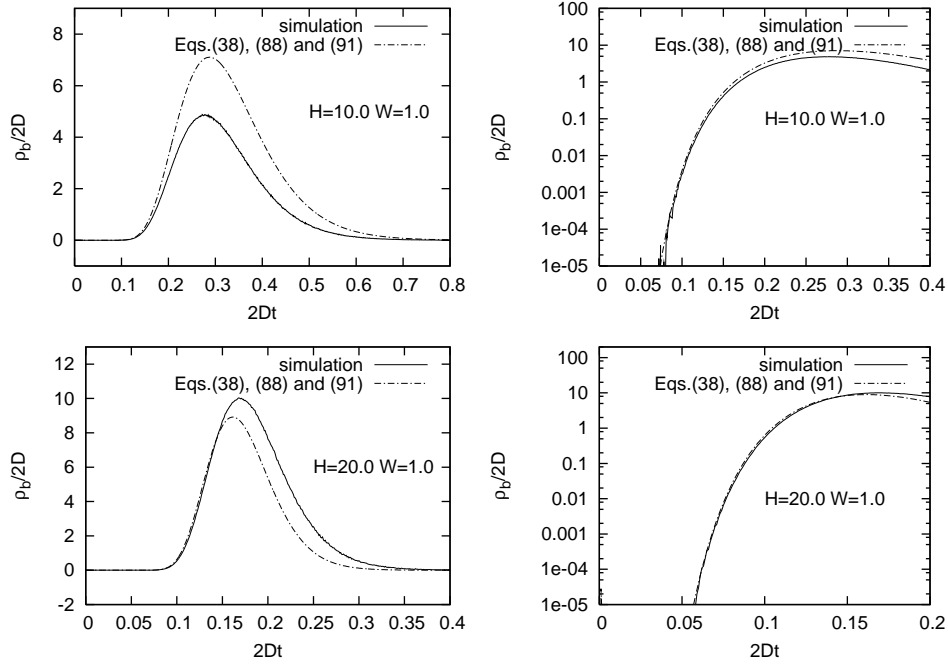


Figure 8: Short time behavior of ρ_b for double-well potentials $U^* = H \left[\left(\frac{x}{W} \right)^2 - 1 \right]$ with two absorbing walls at $-W$ and W , where $W = 1$. Data from path-sampling simulations (solid lines) are compared to numerical estimation of $\rho_b(t \rightarrow 0)$ (dashed lines) based on Eqs.(38), (88) and (91) to numerically estimate the short time behavior of ρ_b .

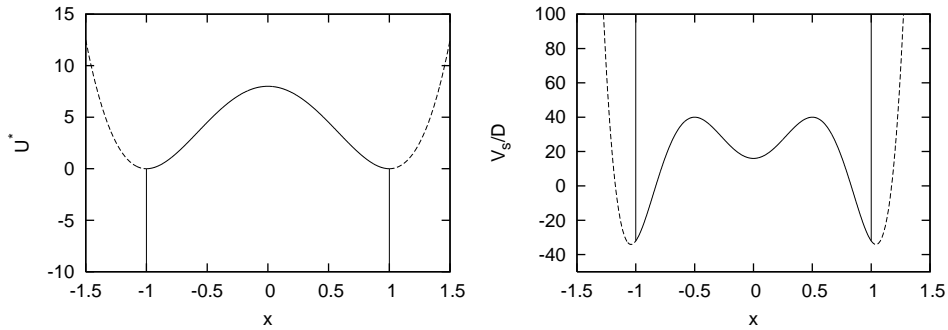


Figure 9: A high barrier double-well potential (left) and its Schrödinger analogue (right) from Eqs.(96) and (97), for $H = 8$ and $W = 1$. The two absorbing walls are put at the two minima. If the barrier height of the potential is not sufficiently large, the minimum of V_s at $x = 0$ will disappear.

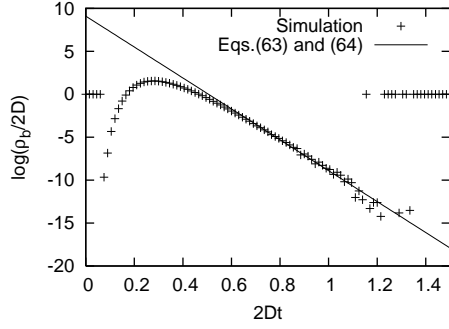


Figure 10: Comparison of two numerical approaches for computing the long time behavior of the event-duration distribution. A path-sampling simulation is compared to pure exponential behavior based on the lowest eigenvalue λ_1 determined from Eqs.(63) and (64) with $H = 10$ and $W = 1$. Similar results are obtained for other high barrier cases.

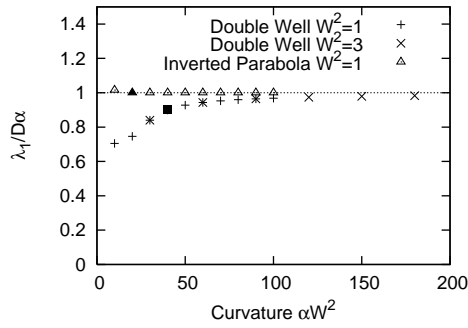


Figure 11: Long time behavior of ρ_b for double-well potentials and the inverted parabola. Exact numerical results for lowest eigenvalue $\lambda_1/D\alpha$ are plotted as a function of the dimensionless curvature αW^2 at the barrier peaks. Note that barrier heights are proportional to α for the models considered. Two double-well potentials with fixed $W^2 = 1$ and $W^2 = 3$, and one inverted parabola system with fixed $W^2 = 1$ are considered. Filled symbols indicate the α values where the barrier height H is 10 (in units of $k_B T$). The values of $\lambda_1/D\alpha$, which dominate the long-time behavior, approach 1 for large curvatures, as predicted by Eq.(107).